International Journal of Pharmaceutics 664 (2024) 124591

Contents lists available at ScienceDirect

International Journal of Pharmaceutics

journal homepage: www.elsevier.com/locate/ijpharm

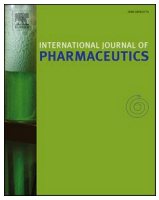

Anticancer drug delivery: Investigating the impacts of viscosity on lipid-based formulations for pulmonary targeting

Anila Mathew Thevarkattil [a], Sakib Yousaf [a], Chahinez Houacine [b], Wasiq Khan [c], Ruba Bnyan [d], Abdelbary Elhissi [e], Iftikhar Khan [a,*]

[a] School of Pharmacy and Biomolecular Sciences, Liverpool John Moores University, Liverpool L3 3AF, United Kingdom
[b] School of Pharmacy and Biomedical Sciences, University of Central Lancashire, Preston PR1 2HE, United Kingdom
[c] Faculty of Engineering and Technology, Liverpool John Moores University, Liverpool L3 3AF, United Kingdom
[d] School of Life Sciences, Pharmacy and Chemistry, Kingston University, London, United Kingdom
[e] Department of Pharmaceutical Sciences, College of Pharmacy, QU Health, Qatar University, P.O. Box 2713, Doha, Qatar

ARTICLE INFO

Keywords:
Viscosity
Lipid-based formulations
Nebulization performance
Sustained release
Nanoparticles

ABSTRACT

Pulmonary drug delivery *via* aerosolization is a non-intrusive method for achieving localized and systemic effects. The aim of this study was to establish the impact of viscosity as a novel aspect (i.e., low, medium and high) using various lipid-based formulations (including liposomes (F1-F3), transfersomes (F4-F6), micelles (F7-F9) and nanostructured lipid carriers (NLCs; F10-F12)) as well as to investigate their impact on *in-vitro* nebulization performance using Trans-resveratrol (TRES) as a model anticancer drug. Based on the physicochemical properties, micelles (F7-F9) elicited the smallest particle size (12–174 nm); additionally, all formulations tested exhibited high entrapment efficiency (>89 %). Through measurement using capillary viscometers, NLC formulations exhibited the highest viscosity (3.35–10.04 m^2/sec). Upon using a rotational rheometer, formulations exhibited shear-thinning (non-Newtonian) behaviour. Air jet and vibrating mesh nebulizers were subsequently employed to assess nebulization performance using an *in-vitro* model. Higher viscosity formulations elicited a prolonged nebulization time. The vibrating mesh nebulizer exhibited significantly higher emitted dose (ED), fine particle fraction (FPF) and fine particle dose (FPD) (up to 97 %, 90 % and 64 μg). Moreover, the *in-vitro* release of TRES was higher at pH 5, demonstrating an alignment of the release profile with the Korsmeyer-Peppas model. Thus, formulations with higher viscosity paired with a vibrating mesh nebulizer were an ideal combination for delivering and targeting peripheral lungs.

1. Introduction

Lung cancer is the second most prevalent cancer in both men and women, accounting for approximately 18 % of cancer-related deaths in developed nations (Siegel et al., 2023). Typically, systemic chemotherapy is offered, which delivers anticancer drugs to non-targeted sites marked by systemic side-effects and poor efficacy (Mangal et al., 2017). Conversely, administration of anticancer drugs *via* inhalation enables the deposition of large concentrations of chemotherapeutic agents directly to the lungs (localized effect), enhancing anti-tumour action and reducing systemic side-effects (Tatsumura et al., 1983).

Pulmonary targeting may be achieved using nanoparticles (NPs) which have been demonstrated to outperform conventional dosage forms in terms of efficacy, reduction in adverse effects and enhanced stability due to their small size, increased surface area and effective targeting (Roa et al., 2011, Yousaf et al., 2021, Subramanian et al., 2016). NPs can be classified into various types based on their composition. The majority of NPs are made from lipids, polymers, proteins and carbohydrates, examples include: liposomes (Elhissi, (2017), Khan et al., 2023, Bnyan et al., 2020), micelles (Andrade et al., 2011), transfersomes (Khan et al., 2021b, Bnyan et al., 2019), dendrimers (Bai et al., 2007), solid lipid nanoparticles (SLNs) (Bai et al., 2007) and nanostructured lipid carriers (NLCs) (Khan et al., 2021a).

Resveratrol (3,5,4́ trihydroxystilbene) a novel anti-cancer agent, is a polyphenol stilbenoid comprising of two phenol rings joined together by ethylene bridges. It exists in two isomeric forms, *cis* and *trans* resveratrol, however the *trans* form (TRES) is considered more biologically active although less stable. It is highly photosensitive and converts to *cis*

* Corresponding author at: School of Pharmacy and Biomolecular Sciences, Liverpool John Moores University, Liverpool L3 3AF, United Kingdom.
E-mail address: I.Khan@ljmu.ac.uk (I. Khan).

https://doi.org/10.1016/j.ijpharm.2024.124591
Received 31 May 2024; Received in revised form 13 August 2024; Accepted 14 August 2024
Available online 19 August 2024

form when exposed to UV and visible light (Neves et al., 1999). Studies have also shown that TRES is unstable at higher pH level and temperature which results in conversion to *cis* form or degradation (Francioso et al., 2014). Additionally, TRES undergoes substantial liver metabolism and has limited water solubility, resulting in low bioavailability (Neves et al., 1999).

It is important to consider the physicochemical properties of NPs and anticancer drugs when developing inhalation formulations as they may affect the drug's residence time in the lungs (Abdulbaqi et al., 2021). Drug loaded NPs are administered to the lungs as a liquid formulation (solution/dispersion) or solid (dry powders) aerosol system *via* dry powder inhalers (DPIs), pressurized metered dose inhalers (pMDIs), nebulizers and soft mist inhalers. pMDIs and soft mist inhalers deliver low drug doses, whereas nebulizers and DPIs can deliver high drug doses typically needed for anticancer drugs to effectively target tumour cells (Rosiere et al., 2019). To ensure effective delivery and prevent issues such as coughing and lung irritation, it is crucial to optimize factors such as pH, viscosity, surface tension and osmolality of the formulations (Labiris and Dolovich, 2003, Cipolla et al., 2013). Hence, an appropriate selection of formulation excipients and nebulizer are key parameters to be considered for optimum outcomes. Deposition of formulations in the lungs takes place by three mechanisms: inertial impaction, sedimentation and diffusion. Particles with an aerodynamic diameter greater than 5 μm deposit by inertial impaction, as they are unable to change their flow track within the airway, hence they deposit in upper respiratory tract. Particles sized between 0.5 and 5 μm deposit through sedimentation in the lower respiratory tract (central and alveolar region). This process yields a notable concentration of fine particles within this region often denoted to as the fine particle fraction (FPF). However, particles under 1 μm deposit by Brownian diffusion in to the peripheral areas of lungs (Darquenne and Prisk, 2004, Khan et al., 2016). In order to understand the mechanism of particle deposition in lungs, the British Pharmacopoeia has recommended an artificial lung model known as the two-stage impinger or twin impinger (TSI). The TSI is comprised of upper and lower stages (with a cut off diameter of 6.4 μm), which mimics the upper and lower respiratory tract and enables the determination of deposited drug into the lungs (Hallworth and Westmoreland, 1987).

In this study, various types of lipid-based formulations: liposomes (F1-F3), transfersomes (F4-F6), micelles (F7-F9), and NLCs (F10-F12) were prepared according to their viscosity (i.e., low, medium and high) by employing different compositions and combinations of phospholipids (SPC), surfactants (Tween 80), solid lipid (glycerol dibehenate; GBD) and liquid lipid (propylene glycol dicaprylate; PGD) using anticancer *trans*-resveratrol (TRES) as the model drug. These formulations were characterized in terms of particle size, drug entrapment, viscosity, and *in-vitro* drug release. The performance of nebulizers was evaluated using a TSI, to deliver the anticancer drug to the pulmonary system. The goal or novelty was to investigate how each formulation's viscosity affected the nebulization performance in terms of nebulization time, sputtering time, mass output and aerosol output rate using two types of nebulizers: air jet and vibrating mesh. Finally, the deposition of TRES in the nebulizer reservoir and stages of TSI were examined to identify the best nebulizer type.

2. Materials and methods

2.1. Materials

Trans-resveratrol (TRES; >97 %) was purchased from Manchester organics, UK. Soybean phosphatidylcholine (SPC; Lipoid S-100; 94 % purity) was acquired from Lipoid, Switzerland. Tween 80 was purchased from Sigma Aldrich, UK. Glycerol dibehenate (GDB; Compritol 888 ATO) was obtained as a free sample from Gattefose, France. Propylene glycol dicaprylate (PGD; Miglyol 840) was a generous gift from Oleo chemicals, UK. Analytical grade ethanol, formic acid (98 %), and HPLC grade acetonitrile (99.8 %) were obtained from Fischer scientific, UK.

2.2. HYPERLINK "SPS:id::Sec1" preparation of liposome formulations

A thin-film method was employed to produce liposomes. Three different formulations (F1, F2 and F3) were prepared (based on their viscosity, i.e., low, medium and high) using three different concentrations of SPC (250, 1500 and 3000 mg), and TRES (50 mg) was employed as the model drug (Table 1). In each liposome formulation, SPC and TRES were dissolved in ethanol (20 mL) using a 100 mL round bottom flask (RBF). The RBF was affixed to a rotary evaporator (Buchi Rotavapor, Switzerland) before being lowered into a water bath previously preheated to 45 °C. A negative pressure was used to evaporate organic solvent at a rotation speed of 270 rpm for 45 min. The RBF was then detached from the rotary evaporator (upon release of negative pressure), the formed thin-film within the RBF was then hydrated with 40 mL of deionized water (DW) and shaken manually for 15 min, followed by 45 min of annealing time (conducted above the phase transition temperature of SPC i.e., −20 °C) to form stable liposomes. In the present work, we have employed deionized water as a medium throughout the experiments in order to simplify the initial stages of formulation development and characterization, thereby allowing more focus on the basic physicochemical properties of the lipid-based formulations. In the literature, many researchers have used deionized water in order to prepare and characterize lipid-based nanocarriers (Chennakesavulu et al., 2018, Chishti et al., 2019, Wang et al., 2013, Amin et al., 2018).

2.3. Preparation of transfersome formulations

Transfersomes were prepared by a thin-film method based upon the method outlined in Section 2.2 using a rotary evaporator. In transfersome formulations, three different formulations (F4, F5, and F6) were prepared based on their viscosity (i.e., low, medium and high) using phospholipid (SPC) and surfactant (Tween 80) in a 1:1 w/w ratio. However, in each formulation (F4, F5 and F6) the concentration of both ingredients was increased (125:125, 750:750 and 1500:1500 mg), simultaneously (Table 1). Transfersome vesicles were formed at 65 °C, which is above the phase transition temperatures of SPC (−20 °C) and

Table 1
Compositions and combinations of lipid-based formulations, where liposome formulations (F1-F3) were prepared using SPC; transfersome formulations (F4-F6) were produced using Tween 80 and SPC in 1:1 w/w ratios; micelles (F7-F9) were formulated using Tween 80; and NLCs (F10-F12) were prepared using Tween 80, solid lipid (glycerol dibehenate (GDB)) and liquid lipid (propylene glycol dicaprylate (PGD)) in 1:1:1 w/w/w ratios. Trans-resveratrol (TRES) (50 mg) was used as a model drug in all formulations.

Formulations	SPC (mg)	Tween 80 (mg)	GDB (mg)	PGD (mg)
Liposomes				
F1	250	–	–	–
F2	1500	–	–	–
F3	3000	–	–	–
Transfersomes				
F4	125	125	–	–
F5	750	750	–	–
F6	1500	1500	–	–
Micelles				
F7	–	250	–	–
F8	–	1500	–	–
F9	–	3000	–	–
NLCs				
F10	–	84	84	84
F11	–	500	500	500
F12	–	1000	1000	1000

Tween 80 (60 °C).

2.4. Preparation of micelle formulations

Micelle formulations (F7, F8 and F9) were prepared regarding their viscosity using a high-pressure homogenization technique. Three different concentrations of Tween 80 (250, 1500 and 3000 mg) were employed, with a constant concentration of TRES (50 mg) (Table 1). To prepare each micelle formulation, two phases were employed: an aqueous phase and a drug phase. The aqueous phase was prepared by adding Tween 80 to 40 mL of DW, which was stirred continuously using a magnetic hotplate (Benchmark scientific, UK) with magnetic stirrer at 600 rpm for 10 min to obtain a uniform dispersion. The drug phase was obtained by dissolving TRES in 3 mL of ethanol, which was then added dropwise into the aqueous phase with continuous stirring for 10 min at 1000 rpm. The resultant mixture was subjected to high-pressure homogenization (IKA T-18, Ultra Turrax digital homogenizer, UK) at 8000 rpm for 3 min, followed by a probe sonication to reduce particle size.

2.5. Preparation of nanostructured lipid carriers (NLCs) formulations

Three different NLC formulations (F10, F11 and F12) were prepared, where the ratios of solid lipid, liquid lipid, and surfactant were maintained constant at 1:1:1 w/w/w, however the concentration of these ingredients varied between formulations (84:84:84 mg (F13), 500:500:500 mg (F14), and 1000:1000:1000 mg (F15)) (based on their visocity; i.e., low, medium, and high) (Table 1). To prepare each formulation, three phases were produced including a lipid phase, an aqueous phase, and a drug phase.

For the hot lipid phase, solid lipid (GDB) was melted above 70 °C using a hotplate along with a liquid lipid (PGD). The aqueous phase contained Tween 80 in 40 mL of DW (preheated to the same temperature as the lipid phase). Whereas in the drug phase, TRES was dissolved in 3 mL of ethanol, which was then added to the preheated lipid phase. Subsequently, the preheated aqueous phase was also poured into the combined/mixed lipid and drug phases. The mixture was then stirred continuously for 15 min at 1200 rpm to obtain a uniform dispersion. The resultant oil in water (o/w) emulsion was subjected to high-pressure homogenization at 10,000 rpm for 3 min, followed by probe sonication. The prepared NLC formulations were allowed to cool down to room temperature to solidify and stabilize the solid lipid in suspension.

2.6. Size reduction using probe sonication method

Vesicle size of lipid-based formulations (F1-F12) was reduced by probe sonication (Qsonica probe sonicator, UK) for a total duration of 9 min (2 min run time and 1 min rest time for 3 cycles) at an amplitude intensity of 60 %. However, the probe sonication procedure may be associated with the leaching of titanium particles in the formulations. As a result, the formulations were subsequently subjected to bench centrifugation (Labnet international centrifuge, USA) for 8 min at 1000 rpm (1250 g) to separate the titanium particles *via* sedimentation, with nanoparticles remaining suspended in the dispersion media.

2.7. Fourier transform infrared spectroscopic (FTIR) analysis

To confirm the physiochemical compatibility between the formulation constituents, FTIR (Agilent Cary 630 FTIR, UK) analysis was performed. To determine the distinctive peaks in the wavelength range of 4000 to 650 cm^{-1} (averaging 16 scan/spectrum), an interferogram between wavenumber and absorbance was constructed and analysed for individual ingredients; TRES, SPC, Tween 80, GDB, PGD, and all formulations (F1-F12).

2.8. Size and zeta potential analysis

Particle size and the polydispersity index (PDI, also referred to as size distribution) of all formulations (F1-F12) were determined by dynamic light scattering *via* a Zetasizer (Malvern Zetasizer nanoseries, UK). The surface charge and the electrophoretic mobility of the vesicles in suspension were measured using a Zetasizer *via* Laser doppler velocimetry.

2.9. Entrapment efficiency of TRES in formulations

The entrapment efficiency of all the tested formulations (F1-F12) was measured by withdrawing 0.5 mL of the formulation into a Millipore filter (Amicon Ultra centrifugal filter (3 kDa), Fischer Scientific, UK), with bench centrifugation conducted for 15 min at 8000 rpm (5900 g). The free or unentrapped drug passed through the Millipore filter and settled as filtrate at the bottom of the tube (unentrapped) which was then analysed *via* HPLC. The entrapped TRES in the vesicle was held by the filter (being too large to pass through the filter unit). For the analysis of the total drug *via* HPLC, 0.5 mL of formulation was dissolved in 4.5 mL of a mobile phase (0.1 % formic acid in DW and acetonitrile (1:1 v/v)). The entrapment efficiency of TRES in formulations was calculated using the following Eq. (1).

$$\text{Entrapment efficiency}\,(\%) = \left(\frac{\text{Total drug} - \text{Unentrapped drug}}{\text{Total drug}}\right) \times 100 \quad (1)$$

A HPLC (Agilent 1200 series instrument, UK) equipped with a UV detector was utilized for quantification of TRES using a wavelength of 306 nm. A mobile phase comprised of 0.1 % formic acid in DW and acetonitrile (1:1 v/v) was used with a flow rate of 1 mL/min. The stationary phase was an Agilent column C18, 5 µm, and 250 mm x 4.6 mm (Agilent Technology, UK). The injection volume was 20 µL, and the temperature of the column was maintained at 25 °C. A calibration curve for TRES in the mobile phase was established in the concentration range of 1–100 µg/mL.

2.10. Rheological analysis

2.10.1. Capillary viscometer

Liquid flow through a capillary under the influence of gravity was measured using Ubbelohde viscometer (U-tube) (VWR, SI Analytics, UK). The viscosity of all formulations (F1-F12) was measured using four types of U-tube viscometers, which differ from each other with respect to their internal capillary diameter at 25 °C. Kinematic viscosity was measured using Eq. (2), where t is the time taken for the liquid to flow, and C is the instrument constant.

$$V\,(m^2/sec) = Ct \quad (2)$$

The instrument constant (C) was calculated by measuring the time taken by a reference liquid of known viscosity (i.e., DW) to flow. The instrument constant, (C) for viscometers A, B, C, and D were 0.003, 0.015, 0.033, and 0.125, respectively. Using kinematic viscosity, it is possible to calculate the dynamic viscosity (Ƞ). It measures the resistance to flow when an external force is applied. Hence, dynamic viscosity was obtained using Eq. (3), where ρ is the density of the liquid.

$$\grave{E}\ (Pa.sec) = C\rho t \quad (3)$$

2.10.2. Rotational viscometer

To determine whether the flow of the liquid follows Newtonian or Non-Newtonian behaviour, the rheological parameter (viscosity as a function of shear rate) was measured at 25 °C. The viscosity of all formulations (F1-F12) was analysed using a stress-controlled rheometer (Discovery HR-10, USA) using a parallel plate attachment. Each formulation was placed between a static bottom plate and a moving geometry, and a shear rate was applied in a linear manner from 1 to 100

sec^{-1} over a span of 60 sec.

2.11. In-vitro aerosolization performance of formulations via nebulization

All formulations (F1-F12) were aerosolized using two nebulizers: a vibrating mesh (Omron Micro-air U22 pocket nebulizer, UK), and an air jet (PARI Turboboy 5 air jet, UK) into a TSI (Gkotsis et al., 2014) (Copley scientific Ltd., Nottingham, UK), where the upper stage represents the upper respiratory tract and the lower stage represents the lower respiratory tract. To collect the aerosol in the TSI, 7 mL of DW was added in the upper stage and 30 mL in the lower stage. Once the TSI had been assembled, the air flow rate was set at 15 L/min with the aid of an air flow meter (Copley scientific Ltd., Nottingham, UK). Pre-nebulization, 3 mL of formulation was placed into the nebulizer reservoir and positioned in front of TSI.

The nebulization performance was assessed in terms of nebulization time, sputtering time, mass output, and aerosol output rate. Nebulization time was established as the time required for continuous aerosol generation until intermittent aerosol generation. Sputtering, on the other hand, is the intermittent generation of aerosol; this duration is determined upon reaching "dryness or until full cessation of aerosol formation". The complete nebulization time was referred to as the sum of nebulization time and sputtering time. The mass output was achieved by calculating the mass difference between the formulation in the nebulizer before and after nebulization. The mass output was determined using the Eq. (4).

$$\text{Mass output}\,(\%) = \left(\frac{\text{Weight of nebulized formulation}}{\text{Weight of formulation present in the nebulizer prior to nebulization}}\right) \times 100 \tag{4}$$

Aerosol output rate was measured gravimetrically by determining the amount/volume of formulation generated per min as shown in Eq. (5).

$$\text{Aerosol output rate}\,(\text{mg/min}) = \left(\frac{\text{Weight of nebulized formulation}}{\text{Complete nebulization time}}\right) \tag{5}$$

Post-nebulization, the deposition of the TRES in the two stages of TSI, as well as the formulation remaining as dead or residual volume in the reservoir was assessed through HPLC. The recovered dose (RD) of the drug is the total amount of drug in the nebulizer reservoir, upper and lower stages. The amount of drug deposited in the upper and lower stages makes up the emitted dose (ED), which is computed as the percentage of RD as shown in Eq. (6).

$$\text{ED}\,(\%) = \left(\frac{\text{Upper stage} + \text{lower stage}}{\text{RD}}\right) \times 100 \tag{6}$$

The concentration of TRES deposited in the lower stage of the TSI was determined *via* fine particle dose (FPD). The fine particle fraction (FPF) was also determined as the percentage of drug deposited in the lower stage of TSI, as shown in Eq. (7).

$$\text{FPF}\,(\%) = \left(\frac{\text{Drug in the lower stage}}{\text{RD}}\right) \times 100 \tag{7}$$

2.12. In-vitro release of TRES from formulations

In order to assess the sustained release behaviour of TRES from the formulations (F1-F12), each formulation was transferred to dialysis bag (3500 Da; Spectra dialysis membrane, USA) submerged in physiological media with aliquots taken from the media at set intervals. The rate of drug release was examined in two different media: acetate buffer (pH 5) and DW (pH 7). In each medium, a combination of co-solvents was used, where methanol (20 %) was additionally included in the release medium to enhance the solubility of TRES. Organic solvent in the dissolution media for in-vitro studies was adopted from the previous study conducted by Nasr et al. (2014) and Khan et al. (2021c), where a hydrophobic drug was employed in lipid-based nanoformulations. The inclusion of methanol ensures that the free drug molecules remain adequately solubilized in the aqueous medium, facilitating their effective diffusion through the dialysis membrane. This approach mitigates the issue of drug precipitation or adsorption on the nanocarrier, thereby providing a reliable assessment of the encapsulation and release efficiencies. From each formulation (F1-F12), a 5 mL aliquot containing 1 mg/mL of TRES was placed in the dialysis bag and positioned in a USP type II dissolution apparatus (Varion, UK), which was immersed in 900 mL of dissolution media (25 °C) at 100 rpm. At 0, 30 min and then 1 hourly intervals, 1 mL aliquots were withdrawn from each media and replaced with 1 mL of freshly prepared media to maintain sink conditions. TRES release study was conducted for 24 hrs and each sample was analysed *via* HPLC. The release study of TRES alone (1 mg/mL) was used as a control to compare the results and to determine its release profile.

2.13. TRES release kinetics

To ascertain the rate and mechanism of drug release from each drug delivery system, dissolution data was employed in various kinetic models. Kinetic studies were carried out using DD Solver. xla (an Add in to MS-Excel) by subjecting the data to zero order (Eq. (8)), first order (Eq. (9), Higuchi model (Eq. (10), and Korsmeyer-Peppas model (Eq. (11) (Costa and Sousa Lobo, 2001, Paarakh et al., 2019).

$$\boldsymbol{Q_t = Q_0 + K_0 t} \tag{8}$$

$$\boldsymbol{Q_t = -K_1 t} \tag{9}$$

$$\boldsymbol{Q_t = Q_0 + K_H t^{0.5}} \tag{10}$$

$$\boldsymbol{Q_t = Q_0 + K_{KP} t^n} \tag{11}$$

where Q_t is the amount of TRES dissolved in time t, Q_0 is the amount of TRES in the medium at time t_0, K_0 is the zero-order rate constant, K_1 is the first order rate constant, K_H is the Higuchi dissolution constant, K_{KP} is the Korsmeyer- Peppas constant, and n is the release exponent. The co-efficient of determination (R^2) was used to assess the best fit for release data. However, R^2 increases as the number of variables increases. Therefore, the adjusted co-efficient of determination (R^2_{adj}) was more acceptable for comparing kinetic models with various number of parameters (Paarakh et al., 2019).

2.14. Statistical analysis

A one-way analysis of variance (ANOVA) or Student's *t*-test was carried out to perform the statistical analysis using SPSS software. This was done to see whether there was any notable difference between any two groups of data or sets of data. A *p*-value less than 0.05 was regarded as statistically significant, and all the data were reported as mean ± SD. All experiments were conducted in triplicate using three different batches.

3. Results and discussions

3.1. FTIR analysis

FTIR spectroscopy was used here specifically to investigate possible interactions between various components of TRES lipid-based formulations, as these interactions are crucial and could potentially impact the stability and effectiveness of formulations. The FTIR of TRES showed characteristic peaks at 3200 cm^{-1}, which represents an OH stretching, a C–C aromatic double bond at 1600 cm^{-1}, a C–C olefin bond at 1580 cm^{-1}, a C-O stretching at 1375 cm^{-1} and a *trans* olefin bond at 963 cm^{-1}. These results are in agreement with early research on IR spectrum of TRES (Bertacche et al., 2006, Moyano-Mendez et al., 2014). The FTIR of SPC and Tween 80 showed symmetrical and asymmetrical stretching bands of CH_2 at 2922 and 2858 cm^{-1}, and bending of C=O group at 1731 cm^{-1} (Ren et al., 2012). Moreover, SPC showed stretching vibrations at 1054 cm^{-1}, which indicated an aliphatic phosphate P=O (PO^{2-}) group (Hou et al., 2021), whereas Tween 80 showed a weak OH stretching vibration at 3496 cm^{-1} (Ren et al., 2012).

The FTIR of formulations (F1-F9) showed spectral changes, which can be seen in Supplementary data (Suppl. SD1). The OH group of TRES at 3200 cm^{-1} overlapped with the OH and CH_2 group of Tween 80 and SPC, and the peaks of TRES at 963 cm^{-1} disappeared due to the interaction of TRES with the PO^{2-} group of SPC. The FTIR of solid lipid (GDB) and liquid lipid (PGD) exhibited a symmetrical and asymmetrical stretching band (CH_2) between 2987 and 2849 cm^{-1}, as well as C=O stretching at 1735 cm^{-1} (Jagdale et al., 2011). Following encapsulation of TRES in NLCs (F10-F12), the C-O stretching of TRES at 1375 cm^{-1} disappeared, and the intensity of OH band increased due to the overlapping of hydroxyl group of TRES with OH group and CH_2 of Tween 80, GDB, and PGD. Formulations (F1-F12) did not exhibit any chemical reactions which led to the formation of new functional groups; therefore, these formulations were observed to be stable.

Table 2
Particle size, polydispersity index (PDI), zeta potential and entrapment efficiency of *trans*-resveratrol (TRES) of formulations (F1-F12). Data are mean ± SD, n = 3.

Formulations	Particle size (nm)	PDI	Zeta potential (mV)	Entrapment efficiency (%)
Liposomes				
F1	140.01 ±9.45	0.34 ±0.10	−16.10±0.10	96.99±0.70
F2	257.23 ±4.24	0.57 ±0.13	−9.76±0.55	97.05±0.63
F3	860.44 ±8.90	1.00 ±0.01	−5.78±0.18	97.54±0.98
Transfersomes				
F4	86.74±1.69	0.06 ±0.01	−13.56±0.60	89.42±1.99
F5	114.60 ±2.10	0.10 ±0.03	−14.26±0.25	96.58±1.65
F6	108.58 ±1.80	0.08 ±0.02	−12.20±0.43	86.90±1.70
Micelles				
F7	173.76 ±7.77	0.36 ±0.12	−16.43±1.19	89.96±4.74
F8	28.93±0.20	0.32 ±0.01	−6.09±1.95	97.57±1.86
F9	12.75±4.13	0.22 ±0.12	−2.25±0.75	98.08±1.72
NLCs				
F10	181.92 ±1.90	0.21 ±0.01	−25.26±0.56	95.75±0.54
F11	214.51 ±8.64	0.42 ±0.02	–23.80±0.72	91.63±3.18
F12	243.13 ±10.13	0.65 ±0.04	−17.10±2.29	93.46±7.53

3.2. Particle size, zeta potential, and entrapment efficiency

Upon analysis, it was noted that as the concentration of lipid and surfactant increased, formulations (F1-F3, and F10-F12) showed an increasing trend in particle size and PDI (Table 2). Liposomes (F1-F3) and NLC formulations (F10-F12) elicited a significantly ($p < 0.05$) larger particle size than the counterpart formulations investigated. The particle size of liposome formulations (F1-F3) increased with increase in SPC concentration due to a greater number of vesicles being formed, which may result in aggregation/collision, resulting in increased viscosity, and hence a higher PDI. These results were in agreement with a study conducted by Wu et al. (2007) where the particle size of papain liposomes increased with an increase in phospholipid concentration. Whereas, an increase in particle size in NLC formulations may be attributed to the high molecular weight of GDB, resulting in complex linkage formation and particle crystallinity in the central core due to their solid nature, contributing to higher viscosity (Barbosa et al., 2016). These results are in agreement with previous studies conducted by Moreno-Sastre et al. (2016), where the incorporation of GDB produced a larger particle size. Conversely, transfersome formulations (F4-F6) were notably smaller in particle size, with a narrow size distribution (Table 2). When Tween 80 was added at low concentrations, they were absorbed by the transfersome membrane in an aqueous solvent (40 mL). As the Tween 80 concentration was increased, the proportion of surfactant molecules in the membrane reached saturation. Above this, the particle size decreased due to the formation of surfactant-lipid mixed micelles, rather than vesicles (López et al., 1998, Lichtenberg et al., 1983, Wu et al., 2007). These findings are in agreement with literature, where an increase in surfactant concentration beyond a threshold value decreases the particle size (Gupta et al., 2012).

One important factor that greatly affects the viscosity and transport capabilities of various nanoparticulate formulations, particularly in pulmonary delivery applications, is the effect of concentration on nanoparticle aggregation in formulations. Higher concentrations of lipid-based nanoparticles can lead to increased aggregation due to enhanced molecular interactions and reduced steric stabilization. This aggregation can result in higher viscosity, affecting the nebulization efficiency and aerosolization performance, which are crucial for aerosol deposition in the “deep lung” (Müller et al., 2002, Das et al., 2011). In our research, NLCs exhibited a complex heterogeneous structure comprising solid and liquid lipids, aggregated at higher concentrations leading to increased viscosity and PDI. On the other hand, liposomes may aggregate at high concentrations due to a greater number of vesicles being formed, hence higher PDI values are generated. Aggregation can alter the particle size distribution, increasing polydispersity and impacting the aerodynamic properties necessary for efficient pulmonary deposition.

The zeta potential of all formulations (F1-F12) was determined to be negatively charged (Table 2), this may be due to the presence of OH^- ions on the surface of the lipid particle gained by the absorption of hydroxyl ions from water (Witayaudom and Klinkesorn, 2017). In addition, the presence of polyphenol compound (such as TRES) or free fatty acids and glycerides in oil (endogenous surface active compound) would produce a negative charge on the particle (Pandita et al., 2014). Drug solubility in the lipid matrix may highly affect the EE and prevent leakage. All formulations (F1-F12) demonstrated high EE (>89 %) ($p > 0.05$), regardless of formulation constituents and viscosity (Table 2).

3.3. Rheological analysis

3.3.1. Capillary viscometer

Viscosity may significantly affect the stability, nebulization performance and drug release profile of lipid vesicles. Upon measuring the

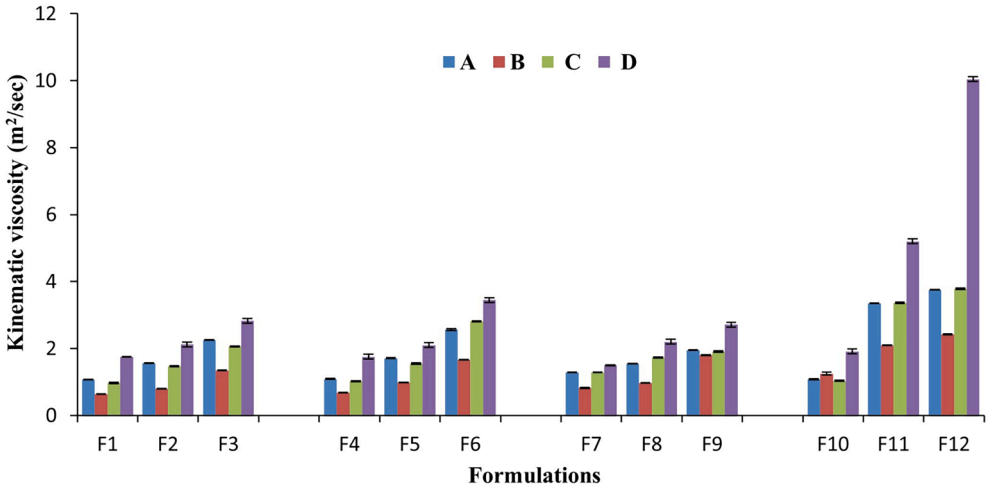

Fig. 1. Kinematic viscosities of all formulations (F1-F12): liposomes (F1-F3), transfersomes (F4-F6), micelles (F7-F9), and NLCs (F10-F12) formulations were determined using four different types of Ubbelohde capillary viscometer (A, B, C and D). Data are mean ± SD, n = 3.

kinematic viscosity of formulations (F1-F12), a proportional relationship was found between viscosity and ingredient concentration (lipids and surfactant) (Fig. 1). This trend was consistently observed in liposome (F1-F3), transfersome (F4-F6) and micelle (F7-F9) formulations, particularly between lower and higher concentrations (Fig. 1). The most prominent difference ($p < 0.05$) was observed in NLC (F10-

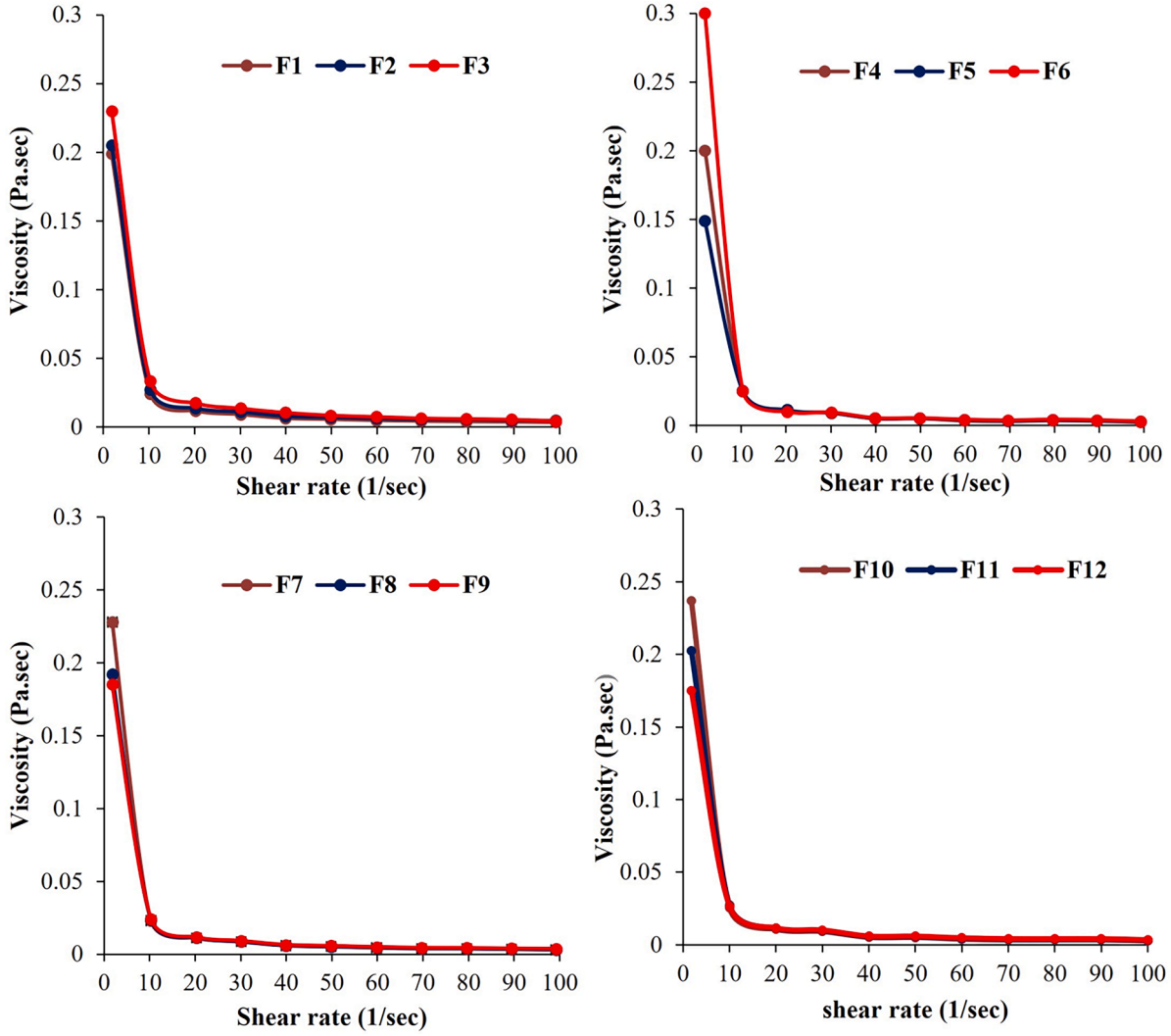

Fig. 2. Flow curves (viscosity versus shear rate) of all formulations: liposomes (F1-F3), transfersomes (F4-F6), micelles (F7-F9), and NLCs (F10-F1) at 25 °C showed a shear-thinning behaviour. Data are mean ± SD, n = 3.

F12) formulations. NLC particles generally consist of a blend of solid and liquid lipids, resulting in a complex and viscous matrix, compared to other vesicular formulations. Chain length of GBD (solid lipid) affects its packing efficiency and crystallinity. Moreover, lipids with longer chain lengths generally lead to more ordered packing and higher viscosity, due to increased molecular interactions and reduced chain mobility. PGD, being in a liquid state at ambient temperatures, forms the surrounding shell or matrix within NLCs. The viscosity contribution of PGD depends on its molecular weight, degree of unsaturation, and the number of NLC particles that resist its flowability. The heterogeneous internal structure of NLCs, characterized by solid lipid cores enveloped in liquid lipid shells, contributes to their elevated viscosity through enhanced molecular interactions and entanglements within the lipid matrix (Müller et al., 2002, Chauhan et al., 2020). Therefore, the data demonstrates that NLC formulations exhibit the highest viscosity, underscoring how their intricate internal architecture distinctly influences their rheological characteristics.

Other lipid-based formulations, like liposomes and transfersomes primarily contain phospholipids, while micelles are composed of amphiphilic surfactant molecules. The composition of these resultant formulations is more uniform and less viscous when compared to NLCs. Liposomes and transfersomes form bilayer vesicles, whereas micelles adopt simpler, spherical structures. These structural differences contribute to lower viscosity due to reduced molecular entanglements and simpler organization (Torchilin, 2007). Differences in viscosity among these formulations are minimal within the experimental margin of error, indicating similar rheological behavior attributed to their straightforward structural organization. Additionally, as the concentration of lipids and surfactant increased, the number of available molecules for bonding also increases proportionally (Sara and Altun, 2021), in turn making them more resistant to flow. Dynamic viscosity of formulations was also calculated from kinematic viscosity. Dynamic viscosity of all formulations (F1-F12) was found to be dependent on formulation density (increase in lipid and surfactant concentration, directly increase density). Hence, the viscosity of lipid-based formulations was ranked as: NLCs > transfersomes > liposomes > micelles.

3.3.2. Rotational viscometer

The fluid properties of formulations (F1-F12) were measured, (i.e., viscosity as a function of shear rate). The relationship between viscosity and shear rate was exhibited as a non-Newtonian (shear-thinning or pseudoplastic) flow behaviour, where the viscosity decreased with increasing shear rate. This behaviour is attributed to the rearrangement in the fluid microstructure in the plane of applied shear (Likavčan et al., 2014) (Fig. 2). However, when the shear rate increased, a point was reached where the viscosity of formulations collapsed abruptly (referred to as yield point), upon further exceeding this value, the viscosity linearly decreased and exhibited Newtonian behaviour. Similar results were also found, where the rheological behaviour of poloxamer gel was studied (Cristiano et al., 2020). The viscosity of formulations was dependent on lipid and surfactant concentrations at different shear rates, and a significant difference ($p < 0.05$) was observed between the lowest and highest concentration of the formulations (Fig. 3). Moreover, a significant difference ($p < 0.05$) in viscosity was also observed between shear rates (i.e., between 10, 50 and 100 sec^{-1}) (Fig. 3). It was found that shear stress impacts the vesicles by changing their size and lamellarity, with the vesicles undergoing conformational changes rather than transition from solid to liquid. Furthermore, formulations exhibited a closely packed structure below their melting temperature, and as the shear rate was exceeded, the flow behaviour became linear, indicating Newtonian behaviour of formulations.

3.4. Nebulization performance

To explore the impact of viscosity on aerosolization performance, all formulations (F1-F12) were evaluated using air jet and vibrating mesh nebulizers (using 3 mL of each formulation).

3.4.1. Nebulization time and sputtering time

Upon analysis, a significantly longer ($p < 0.05$) nebulization time was exhibited by vibrating mesh when compared to the air jet nebulizer (Fig. 4). Nebulization performance (i.e., droplet size, nebulization time) was greatly influenced by formulation viscosity, surface tension and type of ions in the suspension. These impacts interplay with nebulizer design and method of operation (Ghazanfari et al., 2007). Moreover, the influence of viscosity on nebulization time was clearly identified from the vibrating mesh nebulizer. Where, according to the principle of vibrating mesh nebulizer, low energy input for atomization prolonged the nebulization time (Ghazanfari et al., 2007). As formulation viscosity increased, nebulization time increased proportionally (Fig. 4). A significant difference ($p < 0.05$) in terms of nebulization time was noted for air jet nebulizers upon varying viscosity (i.e., low, medium and high) of formulations. Air jet nebulizers may lower the formulation temperature, increasing the formulation viscosity and thus prolonging nebulization time. Formulations may also adhere to the equipment baffle as well as to the side walls of the nebulizer, which increases the time needed to deflect back into the reservoir for re-aerosolization (Khan et al., 2021a). Similar findings were demonstrated by McCallion et al. (1995), Newman et al. (1985) where the nebulization time was prolonged with increase in fluid viscosity using an air jet nebulizer.

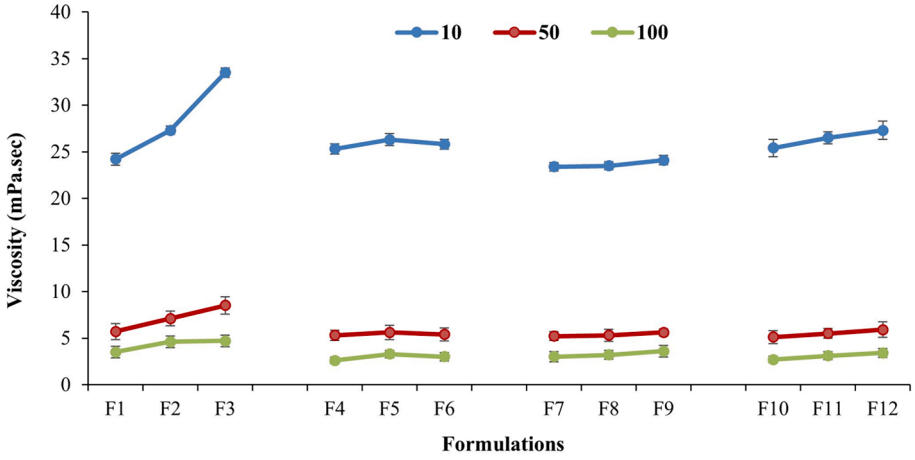

Fig. 3. Viscosity of all formulations, including liposomes (F1-F3), transfersomes (F4-F6), micelles (F7-F9), and NLCs (F10-F12) at different shear rates (10, 50 and 100 *sec*-1) held at 25 °C. Data are mean ± SD, n = 3.

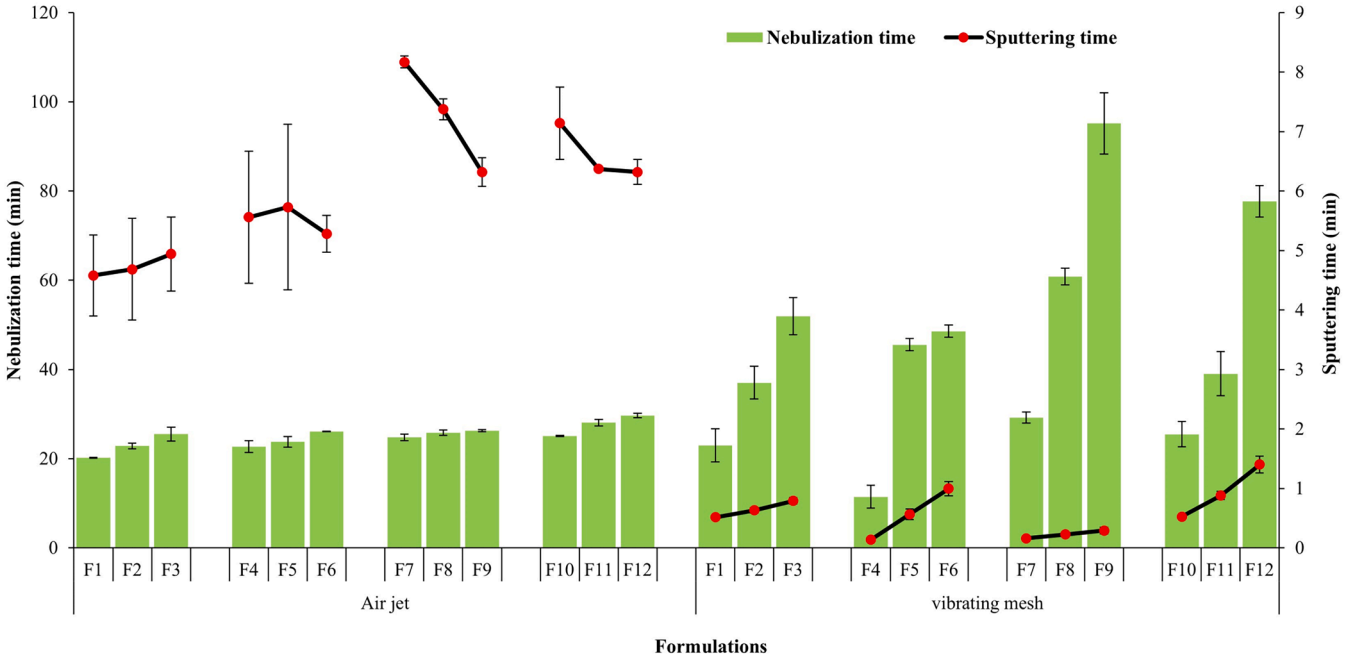

Fig. 4. Nebulization time (vertical bars) and sputtering time (horizontal lines) of TRES-loaded formulations including; liposomes (F1-F3), transfersomes (F4-F6), micelles (F7-F9), and NLCs (F10-F12) were determined using two nebulizers (air jet and vibrating mesh nebulizer). Data are mean ± SD, n = 3.

It was observed that as the viscosity of the formulation increased, both nebulization time and aerosol deposition in the lower impinger stage increased. During nebulization, the liquid formulation is broken down into fine droplets; viscosity influences how quickly droplets detach from the formulation. Formulations with higher viscosity tend to hold onto the liquid more tightly due to their thicker consistency. This results in slower detachment of droplets from the formulation, thereby increasing the nebulization time. This property allows them to form smaller droplets when high shear forces are applied during nebulization and hence greater deposition in the "respirable" fraction is possible (Ghazanfari et al., 2007).

Sputtering time also varied significantly ($p < 0.05$) amongst air jet and vibrating mesh nebulizers (Fig. 4). Significantly higher ($p < 0.05$) sputtering time was demonstrated by the air jet nebulizer, which may be attributed to the adherence of formulations to the internal walls of the nebulizer and baffle, as well as the retention of a large portion of the formulation (known as dead volume or residual volume) in the nebulizer reservoir (extended/prolonged intermittent generation of aerosols). On the other hand, vibrating mesh nebulizers retained a small portion of formulation in the reservoir (due to the slanted design of the reservoir), and therefore a notably short sputtering time was observed.

Thus, a trend of longer nebulization time was observed with increasing viscosity of formulations, regardless of nebulizer type, with a pronounced difference noted between vibration mesh and air jet nebulizers. Moreover, the vibrating mesh nebulizer also exhibited an extremely short sputtering time in comparison to the air jet nebulizer, indicating superiority in compatibility with the nebulized formulations).

3.4.2. Mass output and aerosol output rate

A significantly higher ($p < 0.05$) mass output was exhibited by the vibrating mesh nebulizer in comparison to the air jet nebulizer (Fig. 5). This may be attributed to the nebulizer design, where higher residual volume remained in the reservoir of the air jet nebulizer. Contrastingly, the slanted position of the reservoir in the vibrating mesh nebulizer promoted optimal formulation flow towards the perforated plate for effective aerosolization. This design enhances the generation of aerosols, minimizes formulation retention, and prevents deflection of the formulation back into the reservoir (Khan et al., 2021a). The difference observed in mass output between nebulizer type are supported by previous literature (Elhissi and Taylor, 2005). Mass output exhibited a direct relationship with viscosity, increasing with increased formulation viscosity. These outcomes demonstrate that nebulizer design and formulation physicochemical properties had an impact on mass output.

Aerosol output rate correlated directly with nebulization time; shorter nebulization times were associated with higher aerosol output rates. Therefore, a significantly higher ($p < 0.05$) aerosol output rate was observed for the air jet nebulizer as opposed to the vibrating mesh (Fig. 5). Conversely, the vibrating mesh demonstrated a lower output rate as higher viscosity formulations require longer nebulization times, this has been demonstrated for NLC formulations in previous research (Nafee et al., 2018), along with various other lipid-based formulations (Elhissi et al., 2007). Overall, it was identified that the air jet nebulizer outperformed the vibrating mesh nebulizer in terms of shorter nebulization time, and higher aerosol output rate.

3.4.3. Deposition of TRES in TSI

Post-nebulization, deposition of TRES in the upper and lower stages of TSI (known as ED) and the amount of formulation remaining in the reservoir containing TRES was evaluated. The vibrating mesh nebulizer showed a significantly higher ($p < 0.05$) ED, FPD and FPF than the air jet nebulizer (Table 3). This could be attributed to nebulizer design and formulation viscosity. When using the air jet nebulizer, formulations may adhere/stick to the interior walls of the reservoir, resulting in larger residual volumes within the reservoir (with a shorter nebulization time). Higher residual volumes contribute to the decrease in ED observed, and ultimately lowered the resultant FPD and FPF (delivered into the TSI) (Table 3). Conversely, the vibrating mesh nebulizer exhibited a lower residual volume in the reservoir as the viscosity of the formulation increased, and hence significantly higher ($p < 0.05$) ED, FPD and FPF was achieved. Differences in drop uniformity between both nebulizers employed have been observed when nebulizing liposomal formulations (Elhissi et al., 2013). Moreover, higher FPF was described by Abdelrahim et al. (2010) for vibrating mesh nebulizer using lipid-based formulations.

Upon looking into TRES distribution between nebulizer reservoir and impinger stages, the deposition of TRES in the reservoir of air jet was

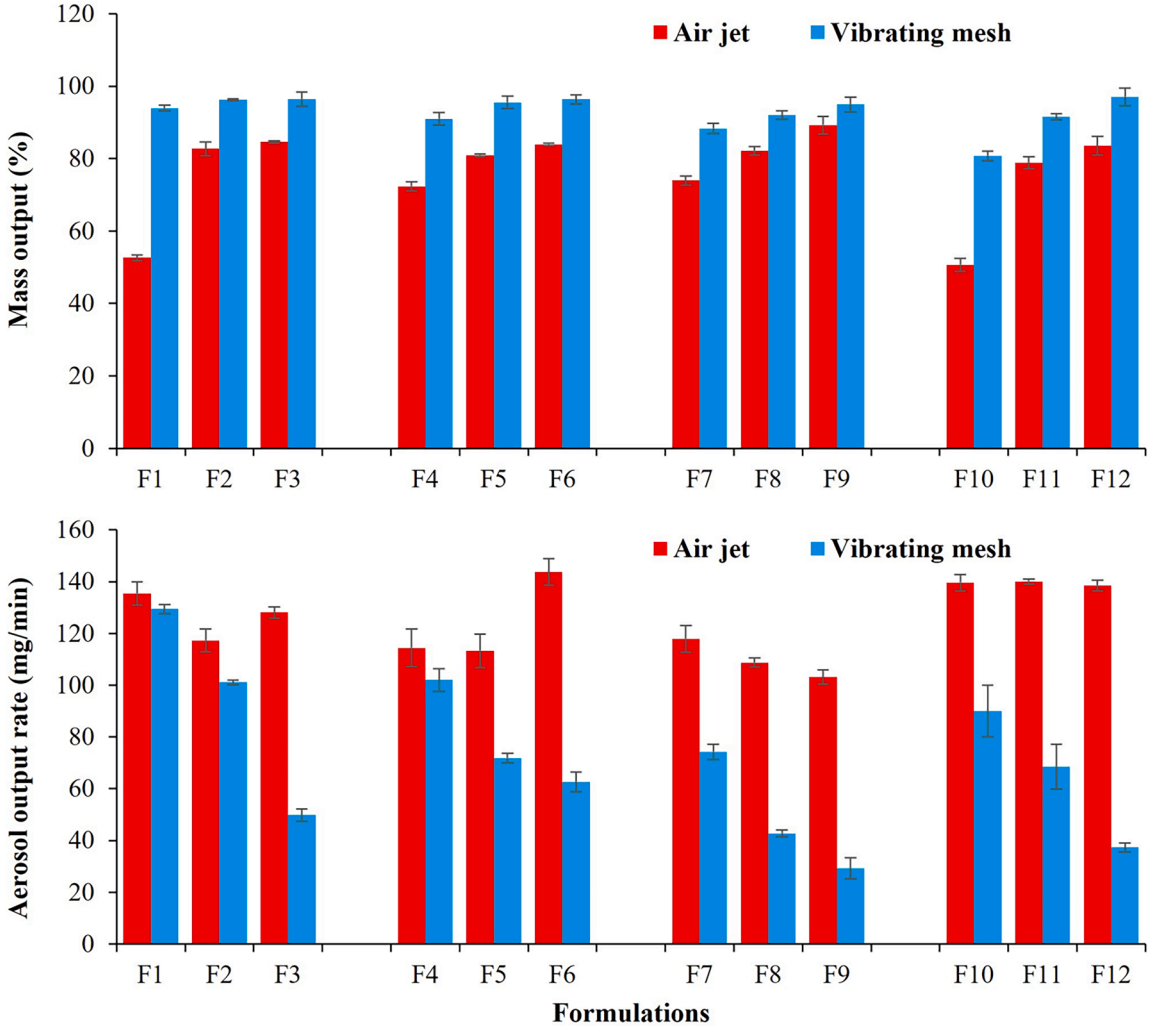

Fig. 5. (A) Mass output, and (B) aerosol output rate of TRES-loaded formulations; liposomes (F1-F3), transfersomes (F4-F6), micelles (F7-F9), and NLCs (F10-F12) were determined using two nebulizers (Air jet and vibrating mesh nebulizer). Data are mean ± SD, n = 3.

Table 3
Nebulization performance of air jet and vibrating mesh nebulizer using liposome formulations (F1-F3), transfersomes (F4-F6), micelles (F7-F9) and NLCs (F10-F12) employing emitted dose (ED), fine particle dose (FPD), and fine particle fraction (FPF) using TSI. Data are mean±SD, n = 3.

Formulation	ED (%)		FPD (μg)		FPF (%)	
	Air jet nebulizer	Vibrating mesh nebulizer	Air jet nebulizer	Vibrating mesh nebulizer	Air jet nebulizer	Vibrating mesh nebulizer
Liposome						
F1	48.76±1.27	78.62±7.92	21.98±0.63	24.55±1.31	44.06±1.42	61.14±4.39
F2	77.11±3.21	91.13±5.42	47.32±0.79	52.43±2.29	70.14±0.53	74.64±3.30
F3	77.97±2.75	93.40±2.24	60.71±1.30	64.68±0.63	71.49±0.89	80.94±5.14
Transfersomes						
F4	62.22±3.76	94.26±0.84	14.88±1.89	18.67±2.50	55.80±2.79	56.99±1.45
F5	74.72±1.7	96.65±0.47	47.55±1.34	53.56±1.58	68.29±1.08	85.25±0.32
F6	77.48±2.71	97.51±0.56	52.39±1.21	59.17±1.49	71.85±1.51	85.60±0.39
Micelles						
F7	68.32±1.60	72.29±1.18	11.75±1.26	12.14±0.35	61.68±4.64	51.76±1.93
F8	82.43±0.61	94.59±0.09	47.24±0.66	51.87±1.92	77.53±0.45	84.56±0.04
F9	85.44±0.71	94.85±0.68	59.48±1.73	64.51±0.98	79.42±0.71	90.47±0.72
NLCs						
F10	43.52±9.20	89.54±1.61	18.09±3.79	25.64±0.53	38.46±5.89	51.24±0.72
F11	72.20±1.92	94.10±1.05	37.46±3.73	46.88±1.74	65.99±4.33	77.55±0.77
F12	76.71±2.11	93.37±3.25	47.28±0.44	57.20±2.19	71.46±5.34	82.16±1.03

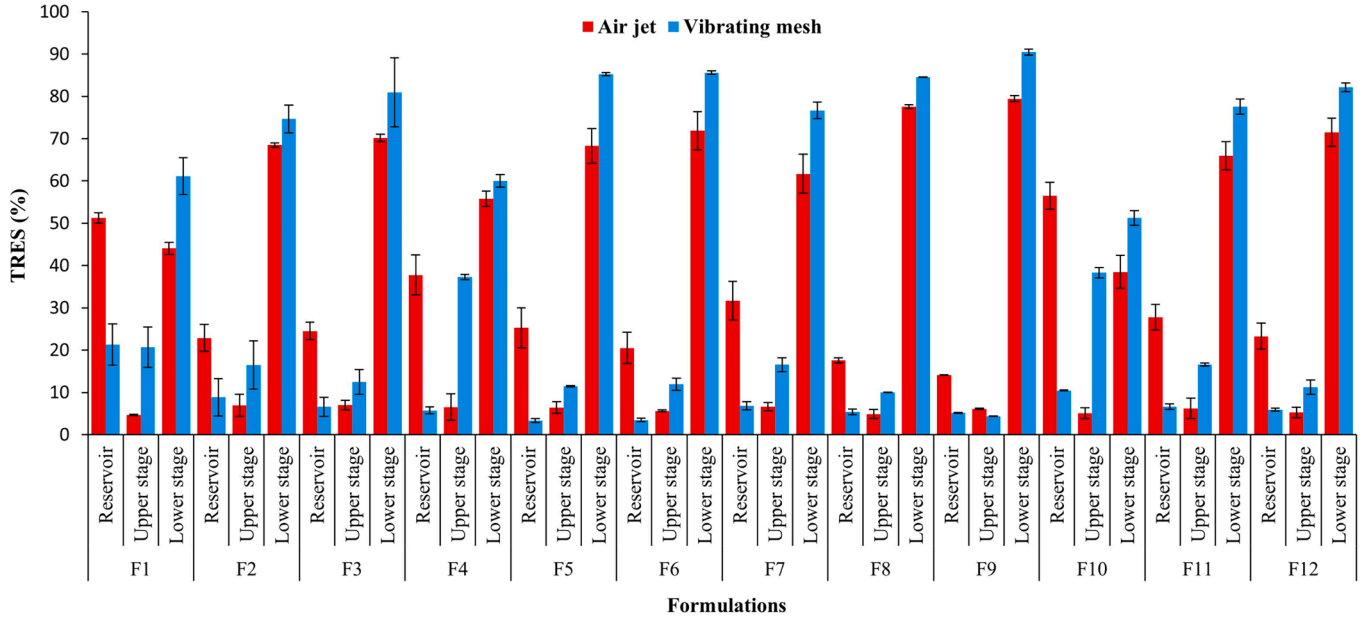

Fig. 6. Deposition of TRES in the nebulizer reservoir, upper and lower stages of TSI: liposomes (F1-F3), transfersomes (F4-F6), micelles (F7-F9) and NLCs (F10-F12) employing two types of nebulizers (air jet and vibrating mesh). Data are mean ± SD, n = 3.

significantly higher ($p < 0.05$) than vibrating mesh nebulizer (Fig. 6). This could be attributed to the aggregation or fusion of the particles in the reservoir due to solvent evaporation caused by compressed gas used during jet nebulization (Clay et al., 1983, Elhissi et al., 2006). Contrastingly, the vibrating mesh nebulizer demonstrated significantly higher ($p < 0.05$) deposition of TRES in the upper stage compared to the air jet nebulizer (Fig. 6). This can be attributed to the larger sized droplets depositing in the upper stage due to inertial impaction. Whilst the vibrating mesh nebulizer produced droplets of uniform size (due to the mesh), plume formation may fuse/adhere some droplets in the air resulting in larger droplets formation. Furthermore, the vibrating mesh nebulizer exhibited significantly higher ($p < 0.05$) TRES deposition in

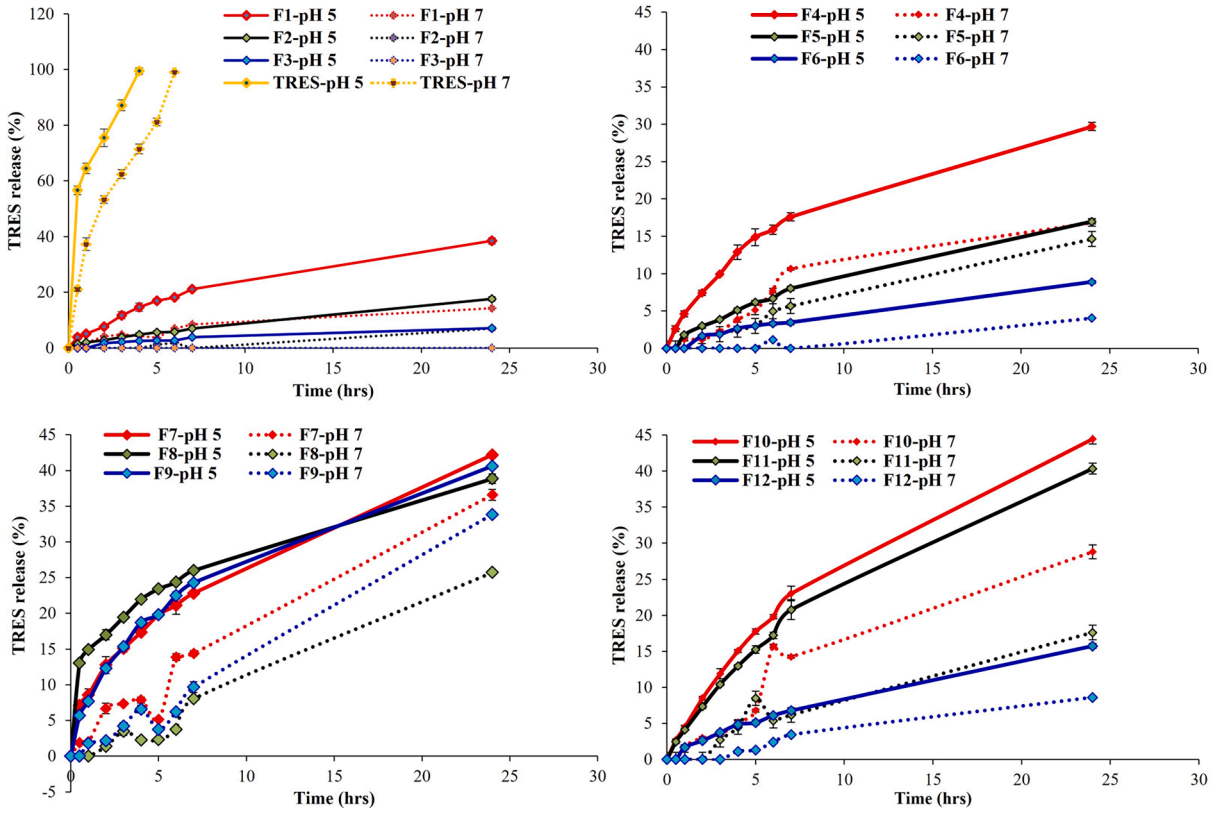

Fig. 7. *In-vitro* release profile of TRES at pH 5 (straight line) and pH 7 (dotted line): TRES as control (Orange colour), liposomes (F1-F3), transfersomes (F4-F6), micelles (F7-F9) and NLCs (F10-F12). Data are mean ± SD, n = 3. (For interpretation of the references to colour in this figure legend, the reader is referred to the web version of this article.)

the lower stage of TSI than air jet nebulizer (due to lower residual volume in the reservoir and a higher mass output) (Fig. 6). Additionally, a significant difference ($p < 0.05$) in TRES deposition in the lower stage of TSI was also observed between formulations prepared with lower and higher viscosities (Fig. 6). Overall, the vibrating mesh nebulizer can be used for successfully targeting the lower respiratory tract (central and alveolar region), in combination with high viscosity formulations achieving higher ED, FPD, and FPF (regardless of formulation type). Overall, as formulation viscosity increased deposition in the lower lung was observed to increase.

3.5. In-vitro release of TRES from formulations

Within 4 h, TRES alone (used as a control) reached 100 % concentration at pH 5 and 70 % at pH 7. All formulations (F1-F12) showed gradual and sustained release of TRES for 24 h in both media. Liposomal formulations (F1-F3) exhibited the lowest and micelles (F7-F9) exhibited the highest drug release regardless of release media (Fig. 7). Upon measuring the drug entrapment using various concentrations of surfactant in micelle formulations, the EE was found to be above 89 %, corresponding to the formation of stable micelle vesicles above their critical micelle concentration (CMC). Moreover, the release study also showed a gradual release of TRES from the nanocarrier. Moreover, various concentrations of a tween 80 surfactant (0–100 μg/ml) were prepared, and their CMC was determined. Each sample was measured using a Sigma 702 Force Tensiometer (Biolin Scientific, UK) using a 50 mm borosilicate cup and a platinum Du Nouy ring. Measurements were conducted in triplicate, and corrections were provided via a Huh-Mason correction. The CMC was calculated based on the tangent and baseline equations, which can be seen in Supplementary data (Suppl. SD2). Based on the evaluation using tween 80 as a surfactant, the CMC was found to be 8.75 μg/ml, which is significantly lower ($p < 0.05$) than the amount of tween 80 employed in micelle formulations (F7-F9). Which may be attributed to the sustained release of TRES from micelle formulations (Fig. 7). The release profile of TRES at pH 5 was significantly higher ($p < 0.05$) than pH 7 (Fig. 7). This may be associated with the higher stability of TRES at lower pH conditions. This is in agreement with findings by Trela and Waterhouse (1996) who observed TRES was stable in acidic medium, with the rate of degradation exponentially increasing with alkaline pH (6.8–9.0).

TRES exhibited stability at acidic pH, which may be related to the presence of OH groups on TRES, protected from radical oxidation by the positively charged H_3O^+ ions (Francioso et al., 2014). Thus, the release of TRES at pH 7 was significantly lower ($p < 0.05$) than at pH 5 (due to the degradation of TRES at this pH), thereby reducing the concentration of TRES in the medium. The degradation of TRES also depends upon the degree of dissociation of hydroxyl groups (i.e., OH group is deprotonated) (Zupančič et al., 2015). An inverse relationship was observed between TRES release and viscosities of formulations (Fig. 7). Successful control over release thus may be achieved by modifying formulation viscosity. Thus, as TRES is stable at pH 5 it can be employed to target the lung, as the pH of the lung is acidic during tumour growth due to excess production of lactic acid.

3.6. TRES release kinetics

Various kinetic models were used to determine the most appropriate and best-fit model for drug release. All formulations (F1-F12) exhibited a strong correlation with the Korsmeyer-Peppas model (Table 4), with no other kinetic models a suitable fit (Suppl. SD3). The R^2_{adj} of Korsmeyer-Peppas was noted in the range of 0.95–0.99 at pH 5 (Table 4), whereas the R^2_{adj} at pH 7 was noted in the range of 0.80–0.98 (Table 4). The release of TRES from the vesicles was identified by the release exponent (n). Where n is ≤ 0.5, the release follows Fickian diffusion (where the diffusion of drug from the matrix/carrier occurs as the liquid penetrates into it). And where n values are greater than 0.5 and lower than 1 (i.e., $0.5 < n < 1$), the release can be considered as non-Fickian or anomalous, where a combination of diffusion as well as erosion may be involved in the release mechanism. The values of n for formulations (F7-F9) at pH 5 were in the range of 0.3–0.5 (Table 4), which represented the Fickian diffusion mechanism of TRES release. However, the other formulations exhibited a non-Fickian release pattern at pH levels of 5 and 7 (Table 4). These results are in agreement with previous results reported by Parsaee et al. (2002), Khan et al. (2021d).

4. Conclusion

The study aimed to examine the influence of formulation viscosity on physicochemical properties and nebulization performance. This impact was evaluated in TSI using both air jet and vibrating mesh nebulizer. Versatile lipid-based formulations (F1-F12) were effectively formulated using different concentrations of phospholipid (SPC), surfactant (Tween 80), solid lipid (GDB), and liquid lipid (PGD). These formulations were adeptly designed for the purpose of pulmonary drug delivery, with the anticancer agent TRES serving as the model drug. Elevating the lipid concentration led to an increase in particle size, although there was a contrasting trend in the case of transfersome formulations. The viscosity profiles of all formulations, measured using both capillary and rotational viscometers, displayed distinct characteristics. When subjected to a capillary viscometer, an elevation in lipid concentration led to higher resistance to flow. Meanwhile, the rotational viscometer revealed non-Newtonian behaviour, where an increase in shear rate reduced the viscosity. Nebulization performance showed that formulations with increased viscosity led to prolonged nebulization time and hence a reduced rate of aerosol output. The mass output from the nebulizers was lower than the total mass initially loaded, indicating the possibility of accumulation or retention of formulation within the nebulizer reservoir. However, the vibrating mesh nebulizer exhibited improved drug distribution in the peripheral areas of the respiratory system (i.e., central and alveolar region) using high viscosity formulations, and displayed

Table 4
Kinetic parameters of Korsmeyer- Peppas model that was fitted to the release of TRES at pH 5 and pH 7: liposomes (F1-F3), transfersomes (F4-F6), micelles (F7-F9) and NLCs (F10-F12).

Kinetic model	Parameters	F1	F2	F3	F4	F5	F6	F7	F8	F9	F10	F11	F12
Korsmeyer- Peppas													
pH 5	kKP	6.434	1.675	0.914	5.963	1.941	0.840	8.923	14.344	9.250	5.345	6.250	1.683
	Rsqr	0.9910	0.9972	0.9582	0.9835	0.9905	0.9809	0.9992	0.9953	0.9938	0.9927	0.9919	0.9930
	Rsqr_adj	0.9899	0.9969	0.9530	0.9815	0.9893	0.9785	0.9991	0.9947	0.9930	0.9918	0.9909	0.9922
	n	0.569	0.740	0.653	0.515	0.687	0.745	0.488	0.308	0.472	0.641	0.623	0.706
pH 7	kKP	2.135	0.043	*	1.718	0.828	0.133	1.943	0.560	1.031	2.530	1.316	0.288
	Rsqr	0.9349	0.9400	*	0.9174	0.9844	0.8167	0.9005	0.9794	0.9862	0.9206	0.9234	0.9563
	Rsqr_adj	0.9267	0.9325	*	0.9070	0.9825	0.7937	0.8880	0.9768	0.9844	0.9106	0.9138	0.9508
	n	0.602	1.602	*	0.733	0.907	1.086	0.656	1.205	1.098	0.776	0.822	1.075

* No TRES release.

elevated ED, FPD, and FPF regardless of formulation type.

CRediT authorship contribution statement

Anila Mathew Thevarkattil: Writing – original draft, Methodology, Formal analysis, Data curation. **Sakib Yousaf:** Writing – review & editing. **Chahinez Houacine:** Visualization, Investigation. **Wasiq Khan:** Software, Resources. **Ruba Bnyan:** Validation, Resources. **Abdelbary Elhissi:** Visualization, Validation. **Iftikhar Khan:** Writing – review & editing, Supervision, Conceptualization.

Declaration of competing interest

The authors declare that they have no known competing financial interests or personal relationships that could have appeared to influence the work reported in this paper.

Data availability

Data will be made available on request.

Acknowledgement

We are very thankful to both Oleo chemicals, UK and Gattefose, France for their generous supply of Propylene glycol dicaprylate (Miglol 840) and Glycerol dibehenate (Compritol 888 ATO).

Appendix A. Supplementary material

Supplementary material to this article can be found online at https://doi.org/10.1016/j.ijpharm.2024.124591.

References

Abdelrahim, M.E., Plant, P., Chrystyn, H., 2010. In-vitro characterisation of the nebulised dose during non-invasive ventilation. J. Pharm. Pharmacol. 62, 966–972.
Abdulbaqi, I.M., Assi, R.A., Yaghmur, A., Darwis, Y., Mohtar, N., Parumasivam, T., Saqallah, F.G., Wahab, H.A., 2021. Pulmonary delivery of anticancer drugs via lipid-based nanocarriers for the treatment of lung cancer: an update. *Pharmaceuticals (Basel)* 14.
Amin, S.G., Shah, D.A., Dave, R.H., 2018. Formulation and evaluation of liposomes of fenofibrate prepared by thin film hydration technique. Int. J. Pharm. Sci. Res 9, 3621–3637.
Andrade, F., Videira, M., Ferreira, D., Sarmento, B., 2011. Micelle-based systems for pulmonary drug delivery and targeting. Drug Deliv. Lett. 1, 171–185.
Bai, S., Thomas, C., Ahsan, F., 2007. Dendrimers as a carrier for pulmonary delivery of enoxaparin, a low-molecular weight heparin. J. Pharm. Sci. 96, 2090–2106.
Barbosa, J.P., Neves, A.R., Silva, A.M., Barbosa, M.A., Salette reis, m. & santos, s. g., 2016. Nanostructured lipid carriers loaded with resveratrol modulate human dendritic cells. Int. J. Nanomed. 11, 3501–3516.
Bertacche, V., Lorenzi, N., Nava, D., Pini, E., Sinico, C., 2006. Host-guest interaction study of resveratrol with natural and modifiedcyclodextrins. J. Incl. Phenom. Macrocycl. Chem. 55, 279–287.
Bnyan, R., Khan, I., Ehtezazi, T., Saleem, I., Gordon, S., O'Neill, F., Roberts, M., 2019. Formulation and optimisation of novel transfersomes for sustained release of local anaesthetic. J. Pharm. Pharmacol. 71, 1508–1519.
Bnyan, R., Cesarini, L., Khan, I., Roberts, M., Ehtezazi, T., 2020. The effect of ethanol evaporation on the properties of inkjet produced liposomes. Daru 28, 271–280.
Chauhan, I., Yasir, M., Verma, M., Singh, A.P., 2020. Nanostructured lipid carriers: a groundbreaking approach for transdermal drug delivery. Adv. Pharm. Bull. 10, 150–165.
Chennakesavulu, S., Mishra, A., Sudheer, A., Sowmya, C., Suryaprakash reddy, C., Bhargav, E., 2018. Pulmonary delivery of liposomal dry powder inhaler formulation for effective treatment of idiopathic pulmonary fibrosis. Asian J. Pharm. Sci. 13, 91–100.
Chishti, N., Jagwani, S., Dhamecha, D., Jalalpure, S., Dehghan, M.H., 2019. Preparation, optimization, and in vivo evaluation of nanoparticle-based formulation for pulmonary delivery of anticancer drug. Medicina 55, 294.
Cipolla, D., Gonda, I., Chan, H.-K., 2013. Liposomal Formulations for Inhalation. *Therapeutic Delivery* 4, 1047–1072.
Clay, M.M., Pavia, D., Newman, S.P., Lennard-Jones, T., Clarke, S.W., 1983. Assessment of jet nebulisers for lung aerosol therapy. Lancet 2, 592–594.
Costa, P., Sousa lobo, J.M., 2001. Modeling and comparison of dissolution profiles. Eur. J. Pharm. Sci. 13, 123–133.
Cristiano, M.C., Froiio, F., Mancuso, A., de Gaetano, F., Ventura, C.A., Fresta, M., Paolino, D., 2020. The Rheolaser Master™ and Kinexus rotational rheometer® to evaluate the influence of topical drug delivery systems on rheological features of topical poloxamer gel. Molecules 25, 1979.
Darquenne, C., Prisk, G.K., 2004. Aerosol deposition in the human respiratory tract breathing air and 80: 20 heliox. J. Aerosol Medicine-Deposition Clear. Effects Lung 17, 278–285.
Das, S., Ng, W.K., Kanaujia, P., Kim, S., Tan, R.B., 2011. Formulation design, preparation and physicochemical characterizations of solid lipid nanoparticles containing a hydrophobic drug: effects of process variables. Colloids Surf. B Biointerf. 88, 483–489.
Elhissi, A., 2017. Liposomes for pulmonary drug delivery: the role of formulation and inhalation device design. Curr. Pharm. Des. 23, 362–372.
Elhissi, A., Brar, J., Najlah, M., Roberts, S., Faheem, A., Taylor, K., 2013. An ethanol-based proliposome technology for enhanced delivery and improved "respirability" of antiasthma aerosols generated using a micropump vibrating-mesh nebulizer. J. Pharma. Technol., Res. Manag. 1, 171–180.
Elhissi, A.M.A., Faizi, M., Naji, W.F., Gill, H.S., Taylor, K.M.G., 2007. Physical stability and aerosol properties of liposomes delivered using an air-jet nebulizer and a novel micropump device with large mesh apertures. Int. J. Pharm. 334, 62–70.
Elhissi, A.M., Karnam, K.K., Danesh-Azari, M.R., Gill, H.S., Taylor, K.M., 2006. Formulations generated from ethanol-based proliposomes for delivery via medical nebulizers. J. Pharm. Pharmacol. 58, 887–894.
Elhissi, A.M.A., Taylor, K.M.G., 2005. Delivery of liposomes generated from proliposomes using air-jet, ultrasonic, and vibrating-mesh nebulisers. J. Drug Delivery Sci. Technol. 15, 261–265.
Francioso, A., Mastromarino, P., Masci, A., D'Erme, M., Mosca, L., 2014. Chemistry, stability and bioavailability of resveratrol. Med. Chem. 10, 237–245.
Ghazanfari, T., Elhissi, A., Ding, Z., Taylor, K., 2007. The influence of fluid physicochemical properties on vibrating-mesh nebulization. Int. J. Pharm. 339, 103–111.
Gkotsis, P.K., Banti, D.C., Peleka, E.N., Zouboulis, A.I., Samaras, P.E., 2014. Fouling issues in membrane bioreactors (MBRs) for wastewater treatment: major mechanisms, prevention and control strategies. Processes 2, 795–866.
Gupta, A., Aggarwal, G., Singla, S., Arora, R., 2012. Transfersomes: a novel vesicular carrier for enhanced transdermal delivery of sertraline: development, characterization, and performance evaluation. Sci. Pharm. 80, 1061–1080.
Hallworth, G.W., Westmoreland, D.G., 1987. The twin impinger: a simple device for assessing the delivery of drugs from metered dose pressurized aerosol inhalers. J. Pharm. Pharmacol. 39, 966–972.
Hou, L., Sun, X., Pan, L., Gu, K., 2021. Effects of phytosterol butyrate ester on the characteristics of soybean phosphatidylcholine liposomes. J. Oleo Sci. 70, 1295–1306.
Jagdale, S., Patil, S., Kuchekar, B., Chabukswar, A., 2011. Preparation and characterization of metformin hydrochloride - compritol 888 ATO solid dispersion. J. Young Pharm. 3, 197–204.
Khan, I., Yousaf, S., Alhnan, M.A., Ahmed, W., Elhissi, A., Jackson, M.J., 2016. Design Characteristics of Inhaler Devices Used for Pulmonary Delivery of Medical Aerosols. In: Ahmed, W., Jackson, M.J. (Eds.), Surgical Tools and Medical Devices. Cham: Springer International Publishing.
Khan, I., Hussein, S., Houacine, C., Khan sadozai, S., Islam, Y., Bnyan, R., Elhissi, A., Yousaf, S., 2021a. Fabrication, characterization and optimization of nanostructured lipid carrier formulations using Beclomethasone dipropionate for pulmonary drug delivery via medical nebulizers. Int. J. Pharm. 598, 120376.
Khan, S., Madni, A., Rahim, M.A., Shah, H., Jabar, A., Khan, M.M., Khan, A., Jan, N., Mahmood, M.A., 2021d. Enhanced in vitro release and permeability of glibenclamide by proliposomes: Development, characterization and histopathological evaluation. J. Drug Delivery Sci. Technol. 63, 102450.
Khan, I., Needham, R., Yousaf, S., Houacine, C., Islam, Y., Bnyan, R., Sadozai, S.K., Elrayess, M.A., Elhissi, A., 2021b. Impact of phospholipids, surfactants and cholesterol selection on the performance of transfersomes vesicles using medical nebulizers for pulmonary drug delivery. J. Drug Delivery Sci. Technol. 66, 102822.
Khan, I., Yousaf, S., Najlah, M., Ahmed, W., Elhissi, A., 2021c. Proliposome powder or tablets for generating inhalable liposomes using a medical nebulizer. J. Pharm. Investig. 51, 61–73.
Khan, I., Al-Hasani, A., Khan, M.H., Khan, A.N., Alam, F.E., Sadozai, S.K., Elhissi, A., Khan, J., Yousaf, S., 2023. Impact of dispersion media and carrier type on spray-dried proliposome powder formulations loaded with beclomethasone dipropionate for their pulmonary drug delivery via a next generation impactor. PLoS One 18, e0281860.
Labiris, N.R., Dolovich, M.B., 2003. Pulmonary drug delivery. Part II: the role of inhalant delivery devices and drug formulations in therapeutic effectiveness of aerosolized medications. Br. J. Clin. Pharmacol. 56, 600–612.
Lichtenberg, D., Robson, R.J., Dennis, E.A., 1983. Solubilization of phospholipids by detergents structural and kinetic aspects. Biochim. Biophys. Acta Rev. Biomembr. 737, 285–304.
LIKAVČAN, L., KOŠÍK, M., BÍLIK, J. & MARTINKOVIČ, M. Determination of Apparent Viscosity as Function of Shear Rate and Fibres Fraction in Polypropylene. 2014.
López, O., de la Maza, A., Coderch, L., López-Iglesias, C., Wehrli, E., Parra, J.L., 1998. Direct formation of mixed micelles in the solubilization of phospholipid liposomes by Triton X-100. FEBS Lett 426, 314–318.
Mangal, S., Gao, W., Li, T., Zhou, Q.T., 2017. Pulmonary delivery of nanoparticle chemotherapy for the treatment of lung cancers: challenges and opportunities. Acta Pharmacol. Sin. 38, 782–797.
McCallion, O.N.M., Taylor, K.M.G., Thomas, M., Taylor, A.J., 1995. Nebulization of fluids of different physicochemical properties with air-jet and ultrasonic nebulizers. Pharma. Res.: Offi. J. Am. Assoc. Pharma. Scient. 12, 1682–1688.

Moreno-Sastre, M., Pastor, M., Esquisabel, A., Sans, E., Viñas, M., Fleischer, A., Palomino, E., Bachiller, D., Pedraz, J.L., 2016. Pulmonary delivery of tobramycin-loaded nanostructured lipid carriers for Pseudomonas aeruginosa infections associated with cystic fibrosis. Int. J. Pharm. 498, 263–273.

Moyano-Mendez, J.R., Fabbrocini, G., de Stefano, D., Mazzella, C., Mayol, L., Scognamiglio, I., Carnuccio, R., Ayala, F., la Rotonda, M.I., de Rosa, G., 2014. Enhanced antioxidant effect of trans-resveratrol: potential of binary systems with polyethylene glycol and cyclodextrin. Drug Dev. Ind. Pharm. 40, 1300–1307.

Müller, R.H., Radtke, M., Wissing, S.A., 2002. Nanostructured lipid matrices for improved microencapsulation of drugs. Int. J. Pharm. 242, 121–128.

Nafee, N., Makled, S., Boraie, N., 2018. Nanostructured lipid carriers versus solid lipid nanoparticles for the potential treatment of pulmonary hypertension via nebulization. Eur. J. Pharm. Sci. 125, 151–162.

Nasr, M., Najlah, M., D'Emanuele, A., Elhissi, A., 2014. PAMAM dendrimers as aerosol drug nanocarriers for pulmonary delivery via nebulization. Int. J. Pharm. 461, 242–250.

Neves, A.R., Lúcio, M., Lima, J.L.C., Reis, S., 1999. Resveratrol in medicinal chemistry: a critical review of its. Food Chem 47, 4456–4461.

Newman, S.P., Pellow, P.G., Clay, M.M., Clarke, S.W., 1985. Evaluation of jet nebulisers for use with gentamicin solution. Thorax 40, 671–676.

Paarakh, M.P., Jose, P.A., Setty, C.M., Christoper, G.V.P., 2019. Release kinetics – concepts and applications. Int. J. Pharm. Res. Technol.

Pandita, D., Kumar, S., Poonia, N., Lather, V., 2014. Solid lipid nanoparticles enhance oral bioavailability of resveratrol, a natural polyphenol. Food Res. Int. 62, 1165–1174.

Parsaee, S., Sarbolouki, M.N., Parnianpour, M., 2002. In-vitro release of diclofenac diethylammonium from lipid-based formulations. Int. J. Pharm. 241, 185–190.

Ren, W., Tian, G., Jian, S., Zhou, L., Yan, L., Jin, S., Yin, W., Zhao, Y., 2012. TWEEN coated NaYF4:Yb, Er/NaYF4 core/shell upconversion nanoparticles for bioimaging and drug delivery. RSC Adv. 2, 7037–7041.

Roa, W.H., Azarmi, S., Al-Hallak, M.K., Finlay, W.H., Magliocco, A.M., Löbenberg, R., 2011. Inhalable nanoparticles, a non-invasive approach to treat lung cancer in a mouse model. J. Control. Release 150, 49–55.

ROSIERE, R., AMIGHI, K. & WAUTHOZ, N. 2019. Nanotechnology-based targeted drug delivery systems for lung cancer: Nanomedicine-based inhalation treatments for lung cancer.

Sara, O.N., Altun, A., 2021. thermal conductivity and viscosity correlations in different kinds of aqueous surfactant solutions at atmospheric pressure as a function of temperature. Int. J. Thermophys. 42.

Siegel, R.L., Miller, K.D., Wagle, N.S., Jemal, A., 2023. Cancer statistics. *CA: A Cancer J. Clini.* 73, 17–48.

Subramanian, S., Khan, I., Korale, O., Alhnan, M.A., Ahmed, W., Najlah, M., Taylor, K.M., Elhissi, A., 2016. A simple approach to predict the stability of phospholipid vesicles to nebulization without performing aerosolization studies. Int. J. Pharm. 502, 18–27.

Tatsumura, T., Yamamoto, K., Murakami, A., Tsuda, M., Sugiyama, S., 1983. New chemotherapeutic method for the treatment of tracheal and bronchial cancers–nebulization chemotherapy. Gan no rinsho. Japan Journal of Cancer Clinics 29, 765–770.

Torchilin, V.P., 2007. Micellar nanocarriers: pharmaceutical perspectives. Pharm. Res. 24, 1–16.

Trela, B.C., Waterhouse, A.L., 1996. Resveratrol: isomeric molar absorptivities and stability. J. Agric. Food Chem. 44, 1253–1257.

Wang, P., Zhang, L., Peng, H., Li, Y., Xiong, J., Xu, Z., 2013. The formulation and delivery of curcumin with solid lipid nanoparticles for the treatment of on non-small cell lung cancer both in vitro and in vivo. Mater. Sci. Eng. C 33, 4802–4808.

Witayaudom, P., Klinkesorn, U., 2017. Effect of surfactant concentration and solidification temperature on the characteristics and stability of nanostructured lipid carrier (NLC) prepared from rambutan (Nephelium lappaceum L.) kernel fat. J. Colloid Interf. Sci. 505, 1082–1092.

Wu, Y., Xu, Y., Sun, W., 2007. Preparation and particle size controlling of papain nanoliposomes. J. Shanghai Jiaotong Univ. Agric. Sci. 25, 105–109.

Yousaf, S.S., Isreb, A., Khan, I., Mewsiga, E., Elhissi, A., Ahmed, W., Alhnan, M.A., 2021. Impact of nanosizing on the formation and characteristics of polymethacrylate films: micro- versus nano-suspensions. Pharm. Dev. Technol. 26, 729–739.

Zupančič, Š., Lavrič, Z., Kristl, J., 2015. Stability and solubility of trans-resveratrol are strongly influenced by pH and temperature. Eur. J. Pharm. Biopharm. 93, 196–204.